This is an open access article published under an ACS AuthorChoice License, which permits copying and redistribution of the article or any adaptations for non-commercial purposes.

ACS OMEGA

http://pubs.acs.org/journal/acsodf

Article

Layer-Dependent Electronic Structure Changes in Transition Metal Dichalcogenides: The Microscopic Origin

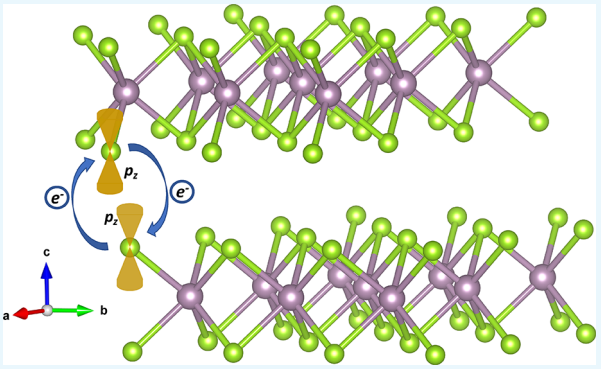
Shishir K. Pandey, Ruma Das, and Priya Mahadevan*

Cite This: *ACS Omega* 2020, 5, 15169−15176

Read Online

ACCESS | Metrics & More | Article Recommendations

ABSTRACT: We have examined the electronic structure evolution in transition metal dichalcogenides MX_2 where M = Mo, W and X = S, Se, and Te. These are generally referred to as van der Waals materials on the one hand, yet one has band gap changes as large as 0.6 eV with thickness in some instances. This does not seem to be consistent with a description where the dominant interactions are van der Waals interactions. Mapping onto a tight binding model allows us to quantify the electronic structure changes, which are found to be dictated solely by interlayer hopping interactions. Different environments that an atom encounters could change the Madelung potential and therefore the onsite energies. This could happen while going from the monolayer to the bilayer as well as in cases where the stackings are different from what is found in 2H structures. These effects are quantitatively found to be negligible, enabling us to quantify the thickness-dependent electronic structure changes as arising from interlayer interactions alone.



INTRODUCTION

Although transition metal dichalcogenides (TMDs) have been studied for more than 50 years, it is amazing that novel phenomena are still being discovered in these materials. Additionally, current efforts for alternate technologies have led to their successful use in catalysis in addition to explorations in photovoltaics, nanoelectronics, etc.[1−5] Analogous to nanomaterials where one finds size dependence of the band gap,[6−8] one finds thickness-dependent changes in the electronic structure of the layered transition metal dichalcogenides.[9−12] Additionally, one finds a thickness-dependent band gap that changes character. The bulk band gap (optical) of MoS_2 is found to be an indirect one of 1.3 eV,[9] which increases to 1.6 eV in the bilayer limit.[10] The nature of the band gap changes and becomes a direct one of 1.9 eV at the monolayer limit.[11] The fact that the monolayers of Mo and W-based transition metal dichalcogenides have a direct band gap (with the exception of WSe_2[13]) is evident from the sharp peak that one finds in the photoluminescence spectra.[14] $MoSe_2$ also has an indirect band gap of 1.1 eV[9] in the bulk limit, whereas, in the monolayer limit, it has a direct band gap of approximately 1.66 eV.[12] A smaller change is found in the band gap of $MoTe_2$ in contrast to MoS_2 and $MoSe_2$.[9] Here, one finds that the indirect bulk band gap of 0.9 eV changes to 1.1 eV at the monolayer limit. Considering the W-based analogues, one has a change of 0.75 eV in WS_2, while one has a smaller change of 0.45 eV in WSe_2.[15−17]

There could be different types of MX_2 (M = Mo, W, Ti, etc., X = S, Se, etc.) sandwiches depending on the coordination of the transition metal atom with the chalcogens as well as the stacking of atoms.[18,19] In this work, we focus our attention on the 2H polymorph of MX_2 (M = Mo, W; X = S, Se, Te)[20−23] where the symmetry about the Mo/W site is trigonal prismatic, though certain generic features are found to be valid across different types of stacking.[19] The bonding within each monolayer is strongly covalent. However, the coupling between layers is believed to be due to weak van der Waals interaction. This has led to the multilayers being called van der Waals homostructures. Hence, the changes in the band gap, which was found to be as large as 0.75 eV in WS_2,[15] seem surprising.

A popular method to examine the size-dependent electronic structure of semiconductor nanostructures has been through the tight-binding model. The size dependence within the model emerges from two effects. The first is the changed coordination of the atom, which could affect the Madelung potential and therefore the onsite energies of the levels of that

Received: March 14, 2020
Accepted: May 27, 2020
Published: June 18, 2020



Downloaded via PEKING UNIV on September 16, 2024 at 10:21:34 (UTC).
See https://pubs.acs.org/sharingguidelines for options on how to legitimately share published articles.

© 2020 American Chemical Society

https://dx.doi.org/10.1021/acsomega.0c01138
ACS Omega 2020, 5, 15169−15176

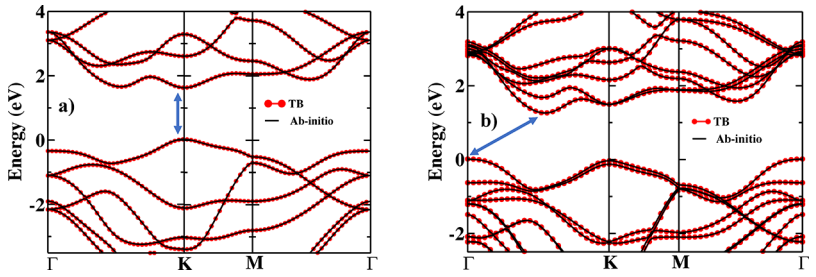


Figure 1. *Ab initio* (solid line) and tight-binding band structures (red circles) for (a) monolayer $MoSe_2$ and (b) bilayer $MoSe_2$. Zero of the energy is the valence band maximum. Arrows represent the VBM and CBM.

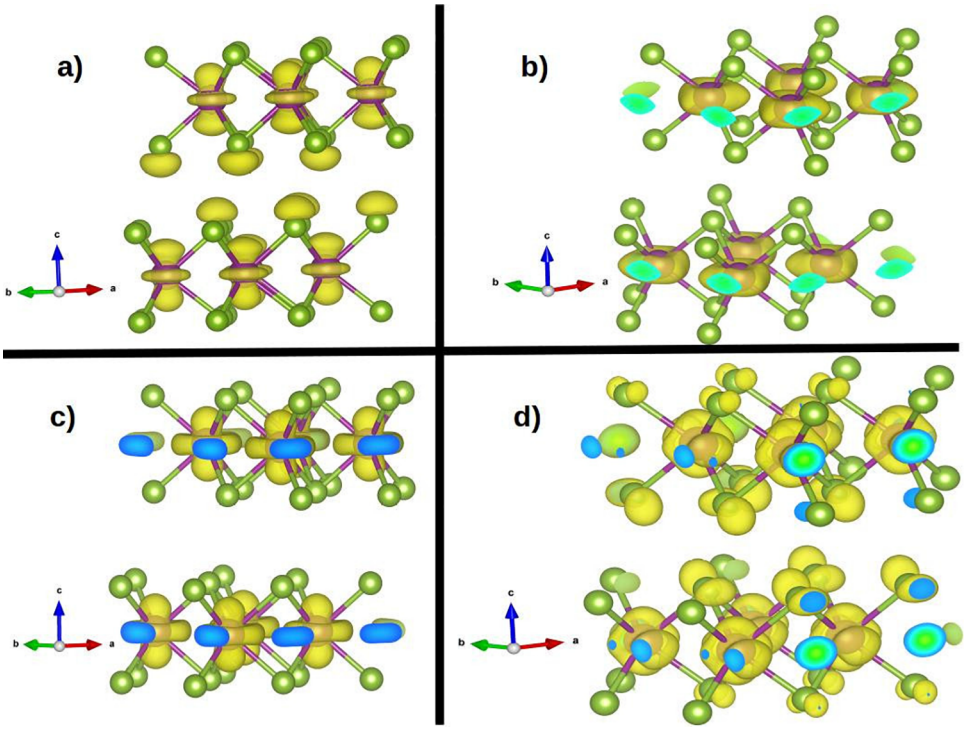


Figure 2. Charge density plots for the (a) highest occupied band at Γ, (b) valence band maximum at *K*, (c) lowest unoccupied band at *T*, and (d) conduction band minimum at *K* for monolayer $MoSe_2$.

atom. The second is the change in the bandwidth due to reduced coordination faced by some of the atoms. Usually, only the latter effects are considered. In the context of transition metal dichalcogenides, however, the effects due to the former become important as, unlike in nanostructures where a small fraction of the atoms has different types of coordination, here, a significant fraction has a coordination different from the bulk. Mapping onto a tight-binding model allows us to explore for the first time the role of various contributions leading to quantum confinement.

The issue of the origin of the size dependence of the band gap in TMDs has been addressed earlier in the literature.[24] Zhang and Zunger[25] examined the electronic structure as a function of thickness and identified the variations seen to arise from two factors: the kinetic energy-controlled quantum confinement and the potential energy-controlled level repulsion. Kang and co-workers[26] suggest that the crystal symmetries of hexagonal-layered materials lead to weak interlayer coupling of the band extrema at the *K* point. Modifications in the local symmetry for instance break these symmetries and allow for the emergence of an electronic structure that depends on thickness. Cappelluti et al.[27] have fit the *ab initio* band structure for a monolayer of MoS_2 to a nearest-neighbor tight-binding model. The same parameters were used for the bilayer with additional interlayer interactions thrown in. This was then used to infer that it is the interlayer interactions that were responsible for the electronic structure changes in MoS_2 with thickness, especially the direct to indirect band gap transition. Among other attempts of tight binding-based studies, there have been a large number of studies determining the relevant tight-binding parameters.[28−31] These studies started with different basis set choices. The values of the parameters entering the tight-binding Hamiltonian were determined either by fitting the *ab initio* band structure in a small energy window in the vicinity of the band gap or constraining the model to reproduce some physical parameters such as the band gap, hole/electron effective mass, and location of the valence band maximum and conduction band minimum. In some instances, a non-orthogonal basis set was used.[28−31] This has the disadvantage in that the extracted onsite energies do not correspond to the natural orbital energy and one cannot discuss trends across the series where the anion is changed for instance. Further, one usually prefers to

https://dx.doi.org/10.1021/acsomega.0c01138
ACS Omega 2020, 5, 15169−15176

work with a model using an orthogonal basis while including many body effects.

We build on the ideas given in the literature. As mentioned earlier, the changed environment could lead to modifications in the Madelung potentials associated with the atoms and consequently changes in the onsite energy. This was not considered earlier. Further, mapping the *ab initio* band structure over a wider range of energy allows us to describe the trends in the electronic structure better. For this reason, we carry out a map of the electronic structure as a function of thickness for Mo- and W-based TMDs. We fixed the interlayer distances at values of which all the calculations are reported in the manuscript and then calculated the electronic structure after switching off the van der Waals interactions. Similar mapping of the *ab initio* band structure onto a tight-binding model was carried out. We find that there is no change in the onsite energies of the bilayers of TMDs from the values that we had including van der Waals interactions. This implies that the van der Waals interactions determine the interlayer separation. However, they do not modify the electronic structure. Additionally, in each of the systems studied, we find that, by switching off the interlayer hopping interactions for the bilayers and beyond, we are able to recover the monolayer band structure. This demonstrates that, even in materials in which the interaction between layers is believed to be of the van der Waals type, it is covalent interactions between the layers that determine the evolution of the electronic structure with an increase in the number of layers. Consequently, knowledge of the tight-binding Hamiltonian for the monolayer as well as the strength of the interlayer hopping interactions allows us to construct the Hamiltonian for any number of layers. While the discussion so far has focused on the stacking that is favored in the bulk structures, the 2H stacking, alternate stackings are also possible. Considering bilayers of $MoSe_2$, steric effects between the electrons on the two layers determine the interlayer separations for different stackings. However, one finds that the nature of stacking has very little effect on the onsite energies, which are again found to be the same as those in the monolayer by similar analysis. These results imply that, even while modeling twisted bilayers of these materials, the variations we find in the electronic structure emerge from the interlayer interactions, which is the approach adopted in the literature. Our analysis in the present work show that the inclusion of weak van der Waals interactions in the Hamiltonian governing the electronic structure does not change the onsite energies and is only responsible for determining the interlayer separation. Building on these arguments, our conclusion that the electronic structure evolution with the number of layers of TMDs is mainly determined by the interlayer hopping interactions stands robust.

RESULTS AND DISCUSSION

The *ab initio* band dispersions for monolayer $MoSe_2$ along various symmetry directions are plotted in Figure 1a. One finds that the valence band maximum (VBM) and the conduction band minimum (CBM) are both located at the *K* point and the system is a direct band gap semiconductor. This is consistent with the experiment, which also finds the system to be a direct band gap semiconductor with a gap of 1.66 eV. While the experimental band gap is the optical band gap,[12] in our calculations, we are calculating the single particle gap. The present calculations that use generalized gradient approximation (GGA) for the exchange correlation functional find a gap of 1.59 eV, which is close to the experimental value. The agreement is however fortuitous as one usually has an underestimation of the band gap due to self-interaction effects

Table 1. Lattice Constants and Plane Wave Energy Cutoffs Considered in Our *Ab Initio* Calculations for the MX_2 Series (M = Mo, W and X = S, Se, and Te)

material	lattice constant (Å)	cutoff energy (eV)
MoS_2	3.150	350
$MoSe_2$	3.289	280
$MoTe_2$	3.519	280
WS_2	3.153	350
WSe_2	3.282	280
WTe_2	3.491	280

Table 2. Onsite Energies Obtained from Tight Binding Mapping of the *Ab Initio* Band Structure[a]

orbitals	monolayer $MoSe_2$	bilayer $MoSe_2$
Se-E_{p_x}	0.00	+0.01
Se-E_{p_y}	0.00	0.0
Se-E_{p_z}	−0.33	−0.38
Mo-$E_{d_{xy}}$	+1.46	+1.51
Mo-$E_{d_{yz}}$	+2.28	+2.31
Mo-$E_{d_{zx}}$	+2.28	+2.31
Mo − $E_{d_{x^2-y^2}}$	+1.46	+1.52
Mo − $E_{d_{z^2}}$	+1.20	+1.27

[a]A basis consisting of Mo d and Se p states was considered for monolayer and bilayer $MoSe_2$. The respective Se p_x is taken as reference for the energies given in eV.

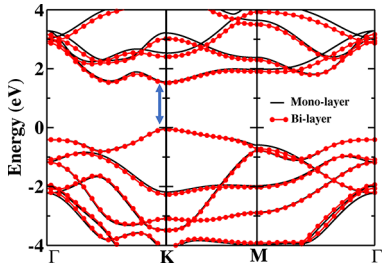


Figure 3. *Ab initio* band structure (solid line) for monolayer $MoSe_2$ compared with the tight-binding band structure (red circles) of the bilayer with interlayer interactions switched off. The zero of energy is the valence band maximum. Arrows represent the VBM and CBM.

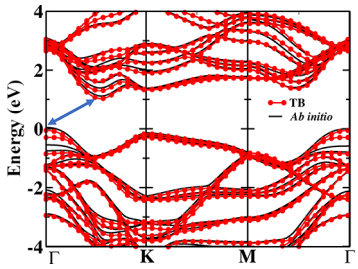


Figure 4. *Ab initio* (solid line) and tight-binding (red circles) band structures for trilayer $MoSe_2$. The tight-binding Hamiltonian for the trilayer has been constructed from the monolayer for the layers and interlayer interactions taken from the bilayer. Zero of energy is the valence band maximum. Arrows represent the VBM and CBM.

https://dx.doi.org/10.1021/acsomega.0c01138
ACS Omega 2020, 5, 15169−15176

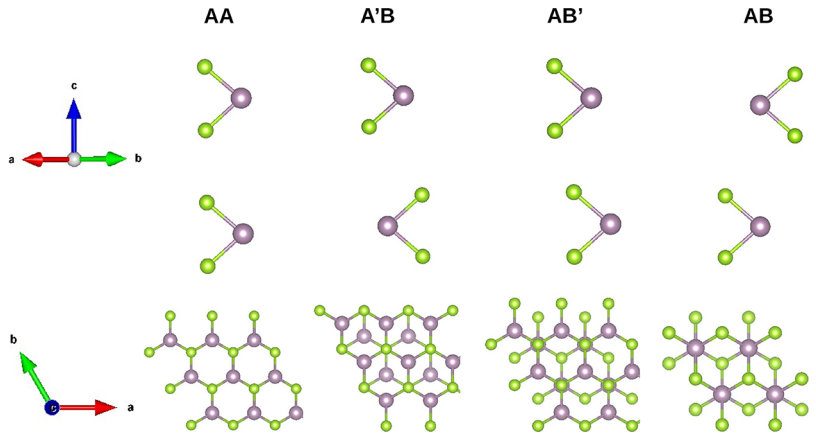


Figure 5. (Colored) Different stackings of TMD bilayers. Violet and green balls are transition metal and chalcogen atoms, respectively.

Table 3. Onsite Energies Obtained from Tight Binding Mapping of the *Ab Initio* Band Structures for Different Stackings of Layers in the $MoSe_2$ Bilayer[a]

orbitals	AA	A′B	AB′	AB
Se-E_{p_x}	0.0	0.0	0.0	0.0
Se-E_{p_y}	0.0	0.0	0.0	0.0
Se-E_{p_z}	−0.35	−0.36	−0.35	−0.35
Mo-$E_{d_{xy}}$	+1.52	+1.53	+1.50	+1.51
Mo-$E_{d_{yz}}$	+2.30	+2.31	2.29	+2.30
Mo-$E_{d_{zx}}$	+2.30	+2.31	2.29	+2.30
Mo − $E_{d_{x^2-y^2}}$	+1.52	+1.53	+1.50	+1.51
Mo − $E_{d_{z^2}}$	+1.28	+1.28	+1.25	+1.26

[a]A basis consisting of Mo d and Se p states was considered. The respective Se p_x is taken as reference for the energies given in eV.

among various other approximations, which use the generalized gradient approximation in the absence of an exact exchange correlation functional. In order to quantify the changes in the electronic structure, we have mapped the *ab initio* band structure onto a tight binding model with Mo d and Se p states in the basis. The tight-binding band structure shown by a red line with circles is superposed on the calculated *ab initio* band structure in Figure 1a. We have a good description of the *ab initio* band structure in the energy window from −3.5 to 4 eV. This gives us confidence in the extracted parameters and allows us to discuss changes in the electronic structure in terms of these parameters.

There are several ways to construct the bilayer of $MoSe_2$. Each monolayer can be visualized as a three-atomic layer

Table 4. Onsite Energies Obtained from Tight Binding Mapping of the *Ab Initio* Band Structure[a]

orbitals	monolayer MoS_2	bilayer MoS_2	BL $MoSe_2$[30]
S-E_{p_x}	0.00	0.0	0.0
S-E_{p_y}	0.00	0.0	0.0
Mo-E_{p_z}	−0.28	−0.25	−0.52
Mo-$E_{d_{xy}}$	+1.66	+1.69	+1.39
Mo-$E_{d_{yz}}$	+2.68	+2.69	+2.36
Mo-$E_{d_{zx}}$	+2.68	+2.69	+2.36
Mo − $E_{d_{x^2-y^2}}$	+1.65	+1.68	+1.39
Mo − $E_{d_{z^2}}$	+1.46	+1.47	+1.15

[a]A basis consisting of Mo d and S p states was considered for monolayer and bilayer MoS_2. The respective S p_x is taken as reference for the energies given in eV. In the fourth column, onsite energies from ref 30 are listed.

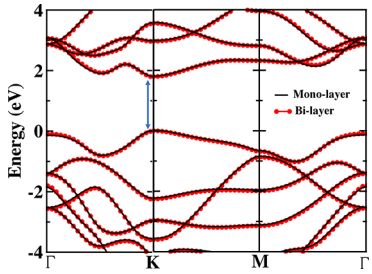


Figure 7. *Ab initio* band structure (solid line) for monolayer MoS_2 compared with the tight-binding band structure (red circles) of the bilayer with interlayer interactions switched off. The zero of energy is the valence band maximum. Arrows represent the VBM and CBM.

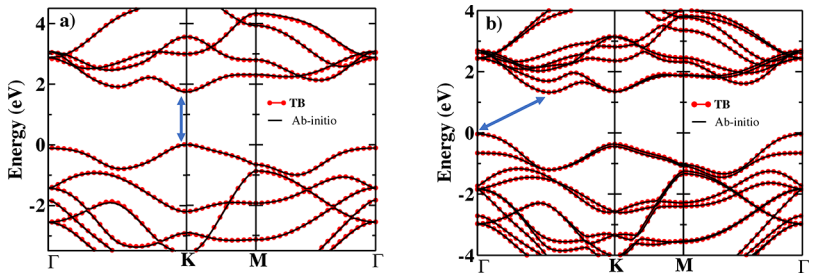


Figure 6. *Ab initio* (solid line) and tight-binding band structures (red circles) for (a) monolayer and (b) bilayer MoS_2. Zero of energy corresponds to the valence band maximum. Arrows represent the VBM and CBM.

https://dx.doi.org/10.1021/acsomega.0c01138
ACS Omega 2020, 5, 15169−15176

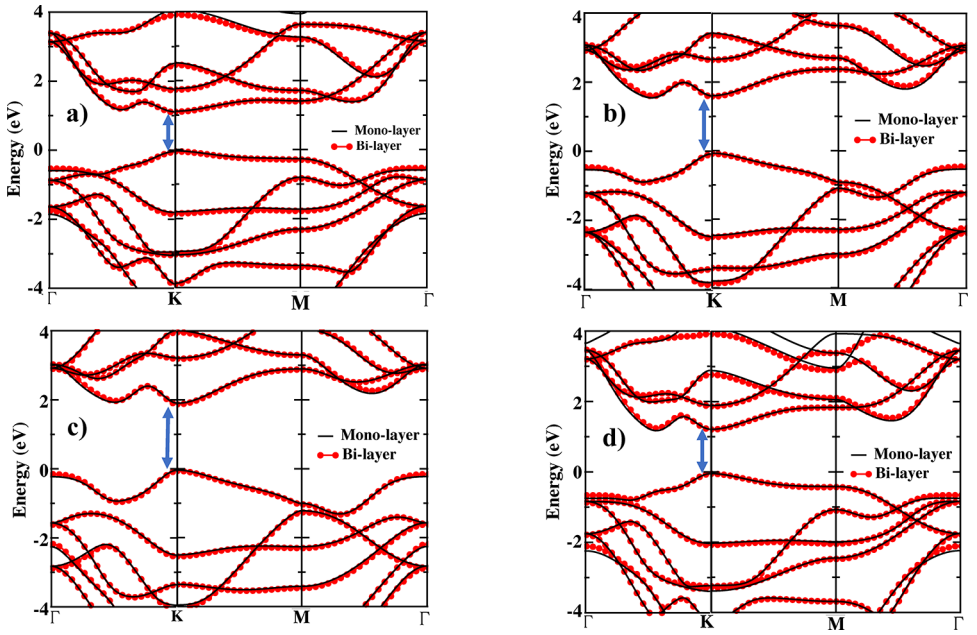


Figure 8. *Ab initio* band structure (solid line) for the monolayer compared with the tight-binding band structure (red circles) of the bilayer with interlayer interactions switched off for (a) $MoTe_2$, (b) WS_2, (c) WSe_2, and (d) WTe_2. The zero of energy is the valence band maximum. Arrows represent the VBM and CBM.

stacking of Mo and Se atoms where Mo atoms are sandwiched between layers of Se atoms. The Se atoms generate a trigonal prismatic crystal field at the Mo site. The stacking that we have considered has the Mo atom in one layer above that in the layer beneath. However, the Mo−Se motif is rotated 180° in the upper layer with respect to the layer beneath. This is referred to as the AA′ stacking and has been shown to have the lowest energy among various stacking patterns considered.[18,19]

Considering a bilayer of $MoSe_2$, we have calculated the band dispersions along various symmetry directions. This is shown in Figure 1b. We find that the VBM, which was at the *K* point, has now shifted to Γ. The CBM is also shifted to the *T* point, which lies along the line from Γ to *K*. This leads to an indirect band gap of 1.25 eV in contrast to the experimental value of 1.55 eV.[10] The changeover in the VBM positions can easily be understood by examining the character of the states contributing to this point. This is shown in Figure 2 where we plot the charge density for the highest occupied band at Γ in panel a.

These are seen to emerge from the interactions between the d_{z^2} orbitals on Mo and p_z orbitals on Se. As these involve orbitals that are directed out of the plane, one finds that these levels in the lower layer interact with the d_{z^2}/p_z orbitals in the layer above. As a result, the highest occupied band at the Γ point moves to higher energies relative to those at the *K* point, and consequently, the VBM shifts to the Γ point when we move from the monolayer to the bilayer. The highest occupied band at the *K* point is contributed by interactions between in-plane orbitals as is evident from Figure 2b. Hence, it shows no shift in the bilayer from its position for the monolayer. Similar analysis of the charge density contributing to the lowest unoccupied band at *T* and *K* symmetry points is shown in Figure 2c,d. We find that in-plane orbitals contribute to the lowest unoccupied band at the *K* point, while out-of-plane orbitals contribute to the lowest unoccupied band at the *T* point. Hence, the increased interaction arising from the presence of the second layer moves the *T* point relative to the *K* point, making the former the conduction band minimum. These ideas are consistent with the analysis of Padilha et al.[32] who examined the movement of various band extrema as a function of the number of layers in MoS_2.

While these ideas are qualitative, we examine the extracted onsite energies and hopping interaction strengths in order to make a more quantitative statement of the role of various effects that determine the electronic structure. As mentioned earlier, we have a good description of the *ab initio* electronic structure within the tight-binding model. This gives us confidence in the extracted parameters. The onsite energies for Se p as well as Mo d orbitals extracted by tight-binding mapping for monolayer as well as bilayer $MoSe_2$ are given in Table 2. In order to understand the role of weak van der Waals interactions on the electronic structure of $MoSe_2$, we first fixed the interlayer separation at the value used for calculations for the bilayer in the manuscript and then switched off the van der Waals interactions. The extracted energies were found to be the same as those given in Table 2 but with a constant shift. It is hence clear from this analysis that the van der Waals term does not modify the Hamiltonian describing the electronic structure of TMDs but enters only the total energy and plays the role of getting the correct interlayer separation in these systems.

After inspection of the onsite energies, one can conclude that the Madelung potential differences for the atoms in the bilayer as compared to the monolayer are very small. This validates the approximation of using the same onsite energies for each layer in several earlier studies in the literature. In order to examine what leads to the differences in the electronic structure in going from the monolayer to the bilayer, we have considered the tight-binding Hamiltonian for the bilayer. All the interlayer interactions have been switched off in this Hamiltonian, and the ensuing band structure has been plotted along various symmetry directions in Figure 3. The band structure for the monolayer has been superposed for comparison. The two band structures look almost identical

https://dx.doi.org/10.1021/acsomega.0c01138
ACS Omega 2020, 5, 15169−15176

suggesting that the only difference between the electronic structure of the monolayer and that for the bilayer emerge from interlayer interactions. The dominant interaction strengths are found between the p_z orbitals of the first (3.72 Å)-neighbor and second (5.92 Å)-neighbor Se atoms.

In order to examine this hypothesis further, we constructed a trilayer of $MoSe_2$. The *ab initio* band structure for the trilayer was calculated along various symmetry directions. This is shown in Figure 4. To compare and examine the hypothesis made vis-à-vis the origin of the changes in the electronic structure as each layer is added, we set up the tight-binding Hamiltonian for the trilayer. This was done by considering the Hamiltonian for the monolayer for each of the layers. The interlayer interactions extracted for the bilayer were then used to couple the layers. The band structure calculated within this model was superposed on the *ab initio* band structure for the trilayer in Figure 4. The comparison is reasonably good, justifying our hypothesis. These results clearly show that the electronic structure changes in going from the monolayer to the bilayer and beyond are derived from interlayer hopping interactions alone.

This is a surprising result as the nomenclature used for these systems is van der Waals structures. This would have us believe that the dominant interaction is van der Waals interactions. However, our analysis suggests that covalent interactions determine the modification in the electronic structure with thickness. This is not entirely surprising as the nearest-neighbor separation between Se atoms of two layers is 3.718 Å. While the nearest neighbor distance of two Se atoms in the same layer is ≃3.289 Å, assuming a Harrison-type scaling law for the distance, one finds that the hopping interaction strengths for the interlayer hopping interaction strengths drop to 70% of the values within the layer. Hence, the presence of finite hopping interaction strengths for electrons in the two layers is not entirely surprising. This immediately raises the question of the role played by van der Waals interactions. This interlayer separation for the bilayer is found to be 3.99 Å when van der Waals interactions are not included and 3.19 Å when they are. Hence, their inclusion merely predicts the interlayer separation.

While we have examined the onsite energies in going from the monolayer to the bilayer for the 2H stacking, there are other stackings possible. In order to examine whether our conclusions were general enough, we considered bilayers with AA, A′B, AB′, and AB stacking, which are shown in Figure 5.[19] As the environment for each atom in the monolayer as well as the bilayer is different in each case, we expect changes in the Madelung potential. In each case, the *ab initio* band structure was fit to a tight-binding model with Mo d and Se p states in the basis. The extracted onsite energies are given in Table 3. These onsite energies for different types of stacking of layers in the $MoSe_2$ bilayer are similar to what we found in the case of 2H stacking (Table 2). Hence, the changed environment for different stackings has very little effect on the onsite energies, and electronic structure changes emerge from the differing interlayer interactions. This is consistent with the approach adopted in the literature to examine the electronic structure of twisted bilayers.[33] Some of the previous studies on twisted bilayer graphene and silicene reported changes in the local density of states in different stacking areas.[34,35]

The evolution of the electronic structure with the number of layers that we find here is not specific to $MoSe_2$ alone. We find similar changes when we examine the electronic structure as a function of the number of layers for MoS_2 also. In Figure 6, we have plotted the *ab initio* band structure for the monolayer in panel a and for the bilayer in panel b. The tight-binding band structure has been superposed in each case, and we have a good description of the *ab initio* band structure. A comparison of the extracted onsite energies is given in Table 4. These extracted values of the onsite energies are in agreement with the values available in the literature.[30]

Here again, we find that the energies for the monolayer and bilayer are similar, as we found earlier. When we considered the tight-binding Hamiltonian for the bilayer and switched off interlayer interactions, we recovered the monolayer band structure. The comparison between the tight-binding Hamiltonian results with interlayer interactions switched off and the *ab initio* band structure for the monolayer is given in Figure 7. In order to demonstrate that the conclusions obtained from our analysis of $MoSe_2$ and MoS_2 are general, we have considered monolayers as well as bilayers of $MoTe_2$, WS_2, WSe_2, and WTe_2. The *ab initio* band dispersions calculated for the monolayer of each of these systems along various symmetry directions are shown in Figure 8. The *ab initio* band structure for the bilayer was mapped onto a tight-binding model with maximally localized Wannier functions for the radial part. The ensuing band structure for the bilayers with interlayer interactions switched off is superposed on the monolayer band structure in Figure 8. The two are found to be almost identical for each of the systems shown here, indicating that the differences in the electronic structure between the monolayer and bilayer arise due to interlayer interactions alone.

CONCLUSIONS

In conclusion, we have examined the evolution in the electronic structure of transition metal dichalcogenides as a function of layers. The changes in the structure that one finds are discussed in terms of a combination of interlayer hopping interactions and Madelung potential effects. In each case, mapping of the *ab initio* electronic structure onto a tight-binding model with transition metal d and anion p states in the basis allows us to quantify the role of each of these effects. Even in these layered materials, which are referred to as van der Waals structures, we find that interlayer hopping interactions play the primary role in bringing about changes in the electronic structure as a function of thickness. On the other hand, we find that expected Madelung potential variations play no role in the observed changes in electronic structure. These ideas are valid across MX_2 where M = Mo, W and X = S, Se, Te. While most results discussed in the manuscript correspond to the 2H stacking, we show that considering other types of stacking does not change the conclusions.

METHODOLOGY

The electronic structure calculations of monolayer and bilayer MX_2 (M = Mo, W; X = S, Se, Te) were carried out within a plane wave implementation of density functional theory (DFT) within VASP[36] (Vienna *ab initio* simulation package). We have taken the 2H stacking of the bilayers in each case as it is found to be the most stable structure.[19] While the lattice constants are kept at the experimental values for the MX_2 series (M = Mo, W; X = S, Se, Te),[20−23] which are listed in Table 1, all the atoms are allowed to relax through a total energy

https://dx.doi.org/10.1021/acsomega.0c01138
ACS Omega 2020, 5, 15169−15176

minimization that is guided by the calculated atomic forces. A vacuum of 20 Å is used along the z direction to minimize the interaction among the periodic images for the monolayer. Projected augmented wave[37,38] potentials are used to solve the electronic structure self-consistently using a k-point mesh of 12 × 12 × 1. Cutoff energies for the plane wave basis states in material series MX_2 (M = Mo, W; X = S, Se, Te) are also listed in Table 1. The Perdew–Burke–Ernzerhof (PBE)[39] approximation was used for the exchange-correlation functional. The weak van der Waals interaction between the layers has an effect in the determination of the interlayer distances. A dispersion correction based on Grimme's DFT-D2 method[40] is used on top of the PBE potentials.

In order to quantify the results, we setup the following tight-binding model with the transition metal d and anion p states in the basis.

$$H = \sum_{i,l} \varepsilon_{\mathrm{d}} \mathrm{d}_{il}^{\dagger}\mathrm{d}_{il} + \sum_{i,l} \varepsilon_{\mathrm{p}} \mathrm{p}_{il}^{\dagger}\mathrm{p}_{il} - \sum_{i,j,l_1,l_2} (t_{i,j,\mathrm{pd}}^{l_1 l_2} \mathrm{d}_{il_1}^{\dagger}\mathrm{p}_{jl_2} + \mathrm{H.\,c.}) - \sum_{i,j,l_1,l_2} (t_{i,j,\mathrm{dd}}^{l_1 l_2} \mathrm{d}_{il_1}^{\dagger}\mathrm{d}_{jl_2} + \mathrm{H.\,c.}) - \sum_{i,j,l_1,l_2} (t_{i,j,\mathrm{pp}}^{l_1 l_2} \mathrm{p}_{il_1}^{\dagger}\mathrm{p}_{jl_2} + \mathrm{H.\,c.})$$

where $\mathrm{d}_{il}^{\dagger}(\mathrm{d}_{il})$ creates (annihilates) an electron in the lth d orbital on the transition metal site in the ith unit cell while $\mathrm{p}_{il}^{\dagger}(\mathrm{p}_{il})$ creates (annihilates) an electron in the lth p orbital on the oxygen atom in the ith unit cell. In this model, the maximally localized Wannier functions[41] are used for the radial parts of the basis functions. Technically, the degree of localization and the symmetry of these Wannier functions can be controlled in the projection procedure. All on-site energies and hopping interaction strengths in this case are determined from the interface of VASP to Wannier90.[42] Once a full tight-binding Hamiltonian is obtained for the bilayers, in order to switch off the interlayer interactions, we identify all the interlayer terms in $t_{i,j,\mathrm{pd}}^{l_1 l_2}\mathrm{d}_{il_1}^{\dagger}\mathrm{p}_{jl_2}$ and $t_{i,j,\mathrm{pp}}^{l_1 l_2}\mathrm{p}_{il_1}^{\dagger}\mathrm{p}_{jl_2}$ and put corresponding t's to zero. Apart from the 2H stacking, for $MoSe_2$, we also explored other stacking geometries, AA, A′B, AB′, and AB shown in Figure 5,[19] to explore the renormalization of the onsite energies due to differing Madelung potentials.

AUTHOR INFORMATION

Corresponding Author

Priya Mahadevan − *Department of Condensed Matter Physics and Material Science, S. N. Bose National Centre for Basic Sciences, Kolkata 700106, India;* orcid.org/0000-0003-0240-4490; Email: priya.mahadevan@gmail.com

Authors

Shishir K. Pandey − *Department of Condensed Matter Physics and Material Science, S. N. Bose National Centre for Basic Sciences, Kolkata 700106, India*

Ruma Das − *Department of Condensed Matter Physics and Material Science, S. N. Bose National Centre for Basic Sciences, Kolkata 700106, India*

Complete contact information is available at: https://pubs.acs.org/10.1021/acsomega.0c01138

Author Contributions

S.K.P. and R.D. contributed equally to this work. Queries should be addressed to priya.mahadevan@gmail.com.

Notes

The authors declare no competing financial interest.

ACKNOWLEDGMENTS

P.M. acknowledges funding from DST-Nanomission, India. The authors thank Poonam Kumari for useful discussions.

REFERENCES

(1) Hu, C.; Yuan, C.; Hong, A.; Guo, M.; Yu, T.; Luo, X. Work function variation of monolayer MoS_2 by nitrogen-doping. *Appl. Phys. Lett.* **2018**, *113*, No. 041602.

(2) Hu, C.; Jiang, Z.; Zhou, W.; Guo, M.; Yu, T.; Luo, X.; Yuan, C. Wafer-Scale Sulfur Vacancy-Rich Monolayer MoS_2 for Massive Hydrogen Production. *J. Phys. Chem. Lett.* **2019**, *10*, 4763−4768.

(3) Feng, Q.; Yan, F.; Luo, W.; Wang, K. Charge trap memory based on few-layer black phosphorus. *Nanoscale* **2016**, *8*, 2686−2692.

(4) Lv, Q.; Yan, F.; Wei, X.; Wang, K. High-Performance, Self-Driven Photodetector Based on Graphene Sandwiched GaSe/WS_2 Heterojunction. *Adv. Opt. Mater.* **2018**, *6*, 1700490.

(5) Wei, X.; Yan, F.; Lv, Q.; Zhu, W.; Hu, C.; Patané, A.; Wang, K. Enhanced Photoresponse in $MoTe_2$ Photodetectors with Asymmetric Graphene Contacts. *Adv. Opt. Mater.* **2019**, *7*, 1900190.

(6) Nanda, J.; Sapra, S.; Sarma, D. D.; Chandrasekharan, N.; Hodes, G. Size-selected Zinc Sulfide Nanocrystallites: Synthesis, Structure and Optical Studies. *Chem. Mater.* **2000**, *12*, 1018−1024.

(7) Ithurria, S.; Tessier, M. D.; Mahler, B.; Lobo, R. P. S. M.; Dubertret, B.; Efros, A. L. Colloidal nanoplatelets with two-dimensional electronic structure. *Nat. Mater.* **2011**, *10*, 936−941.

(8) Viswanatha, R.; Sapra, S.; Satpati, B.; Satyam, P. V.; Dev, B. N.; Sarma, D. D. Understanding the quantum size effects in ZnO nanocrystals. *J. Mater. Chem.* **2004**, *14*, 661−668.

(9) Böker, T.; Severin, R.; Müller, A.; Janowitz, C.; Manzke, R.; Voß, D.; Krüger, P.; Mazur, A.; Pollmann, J. Band structure of MoS_2, $MoSe_2$, and $\alpha - MoTe_2$: Angle-resolved photoelectron spectroscopy and ab initio calculations. *Phys. Rev. B* **2001**, *64*, 235305.

(10) Tongay, S.; Zhou, J.; Ataca, C.; Lo, K.; Matthews, T. S.; Li, J.; Grossman, J. C.; Wu, J. Thermally Driven Crossover from Indirect toward Direct Bandgap in 2D Semiconductors: $MoSe_2$ versus MoS_2. *Nano Lett.* **2012**, *12*, 5576−5580.

(11) Mak, K. F.; Lee, C.; Hone, J.; Shan, J.; Heinz, T. F. Atomically Thin MoS_2: A New Direct-Gap Semiconductor. *Phys. Rev. Lett.* **2010**, *105*, 136805.

(12) Shaw, J. C.; Zhou, H.; Chen, Y.; Weiss, N. O.; Liu, Y.; Huang, Y.; Duan, X. Chemical vapor deposition growth of monolayer $MoSe_2$ nanosheets. *Nano Res.* **2014**, *7*, 511−517.

(13) Zhang, C.; Chen, Y.; Johnson, A.; Li, M.-Y.; Li, L.-J.; Mende, P. C.; Feenstra, R. M.; Shih, C.-K. Probing Critical Point Energies of Transition Metal Dichalcogenides: Surprising Indirect Gap of Single Layer WSe_2. *Nano Lett.* **2015**, *15*, 6494−6500.

(14) Splendiani, A.; Sun, L.; Zhang, Y.; Li, T.; Kim, J.; Chim, C.-Y.; Galli, G.; Wang, F. Emerging Photoluminescence in Monolayer MoS_2. *Nano Lett.* **2010**, *10*, 1271−1275.

(15) Braga, D.; Lezama, I. G.; Berger, H.; Morpurgo, A. F. Quantitative Determination of the Band Gap of WS_2 with Ambipolar Ionic Liquid-Gated Transistors. *Nano Lett.* **2012**, *12*, 5218−5223.

(16) Wilson, J. A.; Yoffe, A. D. The transition metal dichalcogenides discussion and interpretation of the observed optical, electrical and structural properties. *Adv. Phys.* **1969**, *18*, 193−335.

(17) Zhao, W.; Ghorannevis, Z.; Chu, L.; Toh, M.; Kloc, C.; Tan, P.-H.; Eda, G. Evolution of Electronic Structure in Atomically Thin Sheets of WS_2 and WSe_2. *ACS Nano* **2013**, *7*, 791−797.

(18) Chhowalla, M.; Shin, H. S.; Eda, G.; Li, L.-J.; Loh, K. P.; Zhang, H. The chemistry of two-dimensional layered transition metal dichalcogenide nanosheets. *Nat. Chem.* **2013**, *5*, 263−275.

(19) He, J.; Hummer, K.; Franchini, C. Stacking effects on the electronic and optical properties of bilayer transition metal dichalcogenides MoS_2, $MoSe_2$, WS_2, and WSe_2. *Phys. Rev. B* **2014**, *89*, No. 075409.
(20) Bronsema, K. D.; De Boer, J. L.; Jellinek, F. On the structure of molybdenum diselenide and disulfide. *Z. Anorg. Allg. Chem.* **1986**, *540*, 15−17.
(21) Coehoorn, R.; Haas, C.; Dijkstra, J.; Flipse, C. J. F.; de Groot, R. A.; Wold, A. Electronic structure of $MoSe_2$, MoS_2, and WSe_2. I. Band-structure calculations and photoelectron spectroscopy. *Phys. Rev. B* **1987**, *35*, 6195−6202.
(22) Schutte, W. J.; De Boer, J. L.; Jellinek, F. Crystal structures of tungsten disulfide and diselenide. *J. Solid State Chem.* **1987**, *70*, 207−209.
(23) Dawson, W. G.; Bullett, D. W. Electronic structure and crystallography of $MoTe_2$ and WTe_2. *J. Phys. C: Solid State Phys.* **1987**, *20*, 6159−6174.
(24) Kuc, A.; Zibouche, N.; Heine, T. Influence of quantum confinement on the electronic structure of the transition metal sulfide TS_2. *Phys. Rev. B* **2011**, *83*, 245213.
(25) Zhang, L.; Zunger, A. Evolution of Electronic Structure as a Function of Layer Thickness in Group-VIB Transition Metal Dichalcogenides: Emergence of Localization Prototypes. *Nano Lett.* **2015**, *15*, 949−957.
(26) Kang, J.; Zhang, L.; Wei, S.-H. A Unified Understanding of the Thickness-Dependent Bandgap Transition in Hexagonal Two-Dimensional Semiconductors. *J. Phys. Chem. Lett.* **2016**, *7*, 597−602.
(27) Cappelluti, E.; Roldán, R.; Silva-Guillén, J. A.; Ordejón, P.; Guinea, F. Tight-binding model and direct-gap/indirect-gap transition in single-layer and multilayer MoS_2. *Phys. Rev. B* **2013**, *88*, No. 075409.
(28) Rostami, H.; Moghaddam, A. G.; Asgari, R. Effective lattice Hamiltonian for monolayer MoS2: Tailoring electronic structure with perpendicular electric and magnetic fields. *Phys. Rev. B* **2013**, *88*, No. 085440.
(29) Liu, G.-B.; Shan, W.-Y.; Yao, Y.; Yao, W.; Xiao, D. Three-band tight-binding model for monolayers of group-VIB transition metal dichalcogenides. *Phys. Rev. B* **2013**, *88*, No. 085433.
(30) Fang, S.; Defo, R. K.; Shirodkar, S. N.; Lieu, S.; Tritsaris, G. A.; Kaxiras, E. Ab initio tight-binding Hamiltonian for transition metal dichalcogenides. *Phys. Rev. B* **2015**, *92*, 205108.
(31) Zahid, F.; Liu, L.; Zhu, Y.; Wang, J.; Guo, H. A generic tight-binding model for monolayer, bilayer and bulk MoS2. *AIP Adv.* **2013**, *3*, No. 052111.
(32) Padilha, J. E.; Peelaers, H.; Janotti, A.; Van de Walle, C. G. Nature and evolution of the band-edge states in MoS_2: From monolayer to bulk. *Phys. Rev. B* **2014**, *90*, 205420.
(33) Suárez Morell, E.; Correa, J. D.; Vargas, P.; Pacheco, M.; Barticevic, Z. Flat bands in slightly twisted bilayer graphene: Tight-binding calculations. *Phys. Rev. B* **2010**, *82*, 121407.
(34) Zhao, M.; Zhuang, J.; Cheng, Q.; Hao, W.; Du, Y. Moiré-Potential-Induced Band Structure Engineering in Graphene and Silicene. *Small* **2019**, 1903769.
(35) Li, Z.; Zhuang, J.; Wang, L.; Feng, H.; Gao, Q.; Xu, X.; Hao, W.; Wang, X.; Zhang, C.; Wu, K.; Dou, S. X.; Chen, L.; Hu, Z.; Du, Y. Realization of flat band with possible nontrivial topology in electronic Kagome lattice. *Sci. Adv.* **2018**, *4*, No. eaau4511.
(36) Kresse, G.; Furthmüller, J. Efficient iterative schemes for ab initio total-energy calculations using a plane-wave basis set. *Phys. Rev. B* **1996**, *54*, 11169−11186.
(37) Kresse, G.; Joubert, D. From ultrasoft pseudopotentials to the projector augmented-wave method. *Phys. Rev. B* **1999**, *59*, 1758−1775.
(38) Blöchl, P. E. Projector augmented-wave method. *Phys. Rev. B* **1994**, *50*, 17953−17979.
(39) Perdew, J. P.; Burke, K.; Ernzerhof, M. Generalized Gradient Approximation Made Simple. *Phys. Rev. Lett.* **1996**, *77*, 3865−3868.
(40) Grimme, S. Semiempirical GGA-type density functional constructed with a long-range dispersion correction. *J. Comput. Chem.* **2006**, *27*, 1787−1799.
(41) Mostofi, A. A.; Yates, J. R.; Lee, Y.-S.; Souza, I.; Vanderbilt, D.; Marzari, N. wannier90: A tool for obtaining maximally-localised Wannier functions. *Comput. Phys. Commun.* **2008**, *178*, 685−699.
(42) Franchini, C.; Kováčik, R.; Marsman, M.; Murthy, S. S.; He, J.; Ederer, C.; Kresse, G. Maximally localized Wannier functions in $LaMnO_3$ withinPBE + U , hybrid functionals and partially self-consistent GW: an efficient route to construct abinitio tight-binding parameters for e_g perovskites. *J. Phys.: Condens. Matter* **2012**, *24*, 235602.

https://dx.doi.org/10.1021/acsomega.0c01138
ACS Omega 2020, 5, 15169−15176